Well-dispersed Pd−Sn nanocatalyst anchored on TiO_2 nanosheets with enhanced activity and durability for ethanol electarooxidation

Ximei Wang, Wenzhi Fan, Chunmiao Zhang, Mingzhu Chi, Aimei Zhu[*], Qiugen Zhang, Qinglin Liu

Department of Chemical & Biochemical Engineering, College of Chemistry & Chemical Engineering, Xiamen University, Xiamen, 361005, PR China

A R T I C L E   I N F O

A B S T R A C T

Novel Pd_1-Sn_x/TiO_2 nanosheets catalyst with higher activity and durability for ethanol oxidation (EOR) was obtained by $NaBH_4$ co-reduction method in direct ethanol fuel cells (DEFCs). The electrochemical performance tested under alkaline conditions illustrates that the prepared Pd_1−$Sn_{0.6}$/TiO_2 NSs catalyst presents outstanding activity (3381 mA mg_{Pd}^{-1}) and excellent CO anti-poisoning ability for EOR. Meanwhile, the residual current density of Pd_1−$Sn_{0.6}$/TiO_2 NSs nanocatalyst (1207 mA mg_{Pd}^{-1}) is 8.5 times of the Pd/C (JM) catalyst (142 mA mg_{Pd}^{-1}) after the durability test of 5000 s for EOR. Additionally, the Pd_1-Sn_x/TiO_2 nanosheets show prominent electrocatalytic activity in EOR comparison with Pd/TiO_2 nanosheets and Pd−Sn nanocatalysts. Thus, Pd and Sn doped in TiO_2 nanosheets not only display excellent electrocatalytic, but also reduce the cost of Pd, which have some reference value for DEFCs.

1. Introduction

Direct ethanol fuel cells (DEFCs), as low operation temperature power sources for facile handling, storage and transportation, have drawn widespread attention as that their renewable biomass, low noise, non-toxic, and high efficiency [1−5]. So far, Pd has been considered significantly to the evolution of fuel cell catalysis as an efficient noble metal for the alkaline ethanol oxidation reactions [1,6−10]. Nevertheless, the surfaces with unmodified Pd nanoparticles suffer from several major problems, which lead to a sluggish reaction kinetics and serious carbon monoxide (CO) byproduct poisoning with influence on catalytic activity [11−13]. To solve those problems, Pd-based nanoparticles have been prepared through four main approaches: controlling the shape and size, incorporating organic material additives, selecting the proper support materials and adding oxyphile elements in Pd-based catalysts [14−19]. These methods were mainly applied to obtain Pd-based electrocatalysts with large surface area, sufficient activity and long-term electrochemical stability. Meanwhile, Pd-based catalysts have stronger anti CO poisoning ability, which is different from Pt-based catalysts, and it can surmount catalyst poisoning effect in EOR [20−24].

In recent years, Pd-based catalysts with second metals such as Sn [25], Ni [20], Au [26] and Ru [27] or with metal oxides (SnO [28], SnO_2 [29], CeO_2 [30], NiO [31], MgO [31], etc), exhibited more excellent catalytic performance compared to their monometallic counterparts. Some studies manifested that introduction of oxyphilic elements to enhance the catalytic stability were ascribed to the ligand and synergistic effect [19,22]. Among these additives, Sn can furnish oxygen-containing groups to improve the catalytic durability because of the bifunctional mechanism between Sn and Pd [32,33]. Moreover, binding strength of CO−Pd could be weakened by the probable mechanism that the O_2 binding strength to Sn particles was increased due to the electron donation to Pd by Sn nanoparticles [34]. Moreover, there are formation of OH radicals in catalytic process, which can transform CO oxidation into CO_2 [11,35].

Nevertheless, the individual Pd-M (M = Sn, Ni, Ru, Rh, Fe, Au, etc) nanoparticles easily aggregate [36,37], which dramatically decreases the utilization efficiency of Pd-M and thus the active sites of the catalyst cannot be fully utilized. To overcome this issue, preparation of highly dispersed and narrow particle size nanoparticles by different methods such as Microwave method, ultrasonic irradiation, electrodeposition reduction, etc [36,38−40]. Unfortunately, the synthesis methods mentioned above make them

* Corresponding author.
  E-mail addresses: 877863921@qq.com (X. Wang), fanwenzhi940504@gmail.com (W. Fan), 2032215505@qq.com (C. Zhang), 1285336209@qq.com (M. Chi), amzhu@xmu.edu.cn (A. Zhu), qgzhang@xmu.edu.cn (Q. Zhang), qlliu@xmu.edu.cn (Q. Liu).

hard to large-scale applications. Although the catalyst nano-composites can be obtained using the co-reduction method, the catalyst aggregation is still unavoidable. Besides, it is possible to solve the catalyst aggregation and intolerable cost problems by selecting a suitable carrier (high surface areas, thermal conductivity and good chemical durability). It is well known that there are different degrees of carbon corrosion for all carbon materials, resulting in the deactivation of the catalyst. Therefore, it is important to look for a non-carbonaceous carrier to solve corrosion problem. In a recent study, metal oxides (SiO_2 [41], CeO_2 [30], TiO_2 [42], etc) are used as catalyst carriers, among which TiO_2 has stronger corrosion resistance ability and higher mechanical strength than conventional carbon black, and may play vital role in the catalytic process to provide oxygen-containing substances and fascinating chemical stability [43–45]. Unique two-dimensional TiO_2 nanosheets (TiO_2 NSs) are one of the primary conditions for the preparation of high-efficiency electrocatalysts as a carrier of immobilizing metal nanoparticles. And it is cheaper than the un-modified two-dimensional material graphene, and the preparation method is simpler [12]. Otherwise, previous research showed that the (001) surface of TiO_2 has more efficient active sites than the thermodynamically stable (101) surface [46–49]. In recent years, anatase TiO_2 nanocrystals/nanosheets with unique two-dimensional structure, which has more exposed high energy (001) patches, have been successfully formed in different reaction systems by using hydrofluoric acid as a capping agent [45,47]. Therefore, the partial anchoring of Pd and Sn with TiO_2 NSs is helpful to enhance the adsorption CO_2 and the band energy CO—Pd can be weakened to obtain excellent electrocatalytic performance [7,8].

Herein, a facile and general approach is developed for load bimetallic Pd—Sn nanoparticles on two-dimensional TiO_2 NSs. The Pd—Sn/TiO_2 NSs catalysts with different proportion of precursors were prepared by in-situ chemical reduction of $PdCl_2$ and $SnCl_2$ on TiO_2 NSs. Compared to the Pd—Sn, Pd/TiO_2 NSs and Pd/C (JM), the Pd—Sn/TiO_2 NSs exhibit substantially enhanced activity and stability for EOR.

2. Preparation of catalysts

Fig. 1 shows the synthesis progress of Pd—Sn/TiO_2 nanosheets, which mainly includes functional TiO_2 nanosheets synthesis, Pd and Sn nanoparticles in-site reduction anchored on TiO_2 nanosheets.

At first, the TiO_2 nanosheets (TiO_2 NSs) were obtained according to the reported procedures [48–50]. TBOT (5 mL) and HF (2 mL) were added with high-pressure reaction kettle (20 mL) after stirring for 1 h, then 5 mL of ethanol (Et) solution was slowly added dropwise into the above solution. The mixed solution was stirred magnetically for 30 min, then transferred to the oven and reacted at 180 °C for 16 h.

Secondly, the NH_2-functionalized TiO_2 NSs precursors (f-TiO_2 NSs) were prepared according to references [47,48]. TiO_2 NSs (56 mg) were dispersed in ethanol (32 mL) after 2 h ultrasonic treatment. Then reacted with H_2O (2 mL), ammonium hydroxide (2 mL) and 3-Aminopropyltromethoxysilane (APTMS, 1.4 mL) for 12 h.

At last, the Pd—Sn/TiO_2 nanosheets were obtained by $PdCl_2$ and $SnCl_2$ co-reduced on f-TiO_2 nanosheets. The f-TiO_2 NSs (10 mg) were dispersed in EG (10 mL) under sonication, and $PdCl_2$ (0.5 mL, 0.09 M) and $SnCl_2$ (1.5 mL, 0.0189 M) were added synchronously. Then, 0.5 M NaOH/EG rapidly adjust the pH of the mixed solution so that the value of pH is 10–10.5, followed by slowly adding 25 mL $NaBH_4$ (2.0 mg mL^{-1}). Then the solution was stirred at room temperature for 8 h. Finally, the Pd—Sn/TiO_2 nanosheets were centrifuged and washed repeatedly with ethanol and ultrapure water. The dry products (4 mg) were dispersed in 2 mL ultrapure water to obtain a certain concentration of catalyst.

Pd—Sn/TiO_2 nanosheets with different Pd/Sn ratios were obtained by controlling the amount of $SnCl_2$ and keeping the amount of $PdCl_2$ unchanged. The weight percent of Pd is around 22.30% for as-prepared Pd_1-Sn_x/TiO_2 NSs, while the weight percent of Sn for Pd_1—$Sn_{0.25}$/TiO_2 NSs, Pd_1—$Sn_{0.6}$/TiO_2 NSs and Pd_1—Sn_1/TiO_2 NSs catalysts is about 5.58%, 13.38% and 22.30%, respectively. At the same time, supplementary materials show the details of materials for catalysts preparation, physical and chemical characterization of
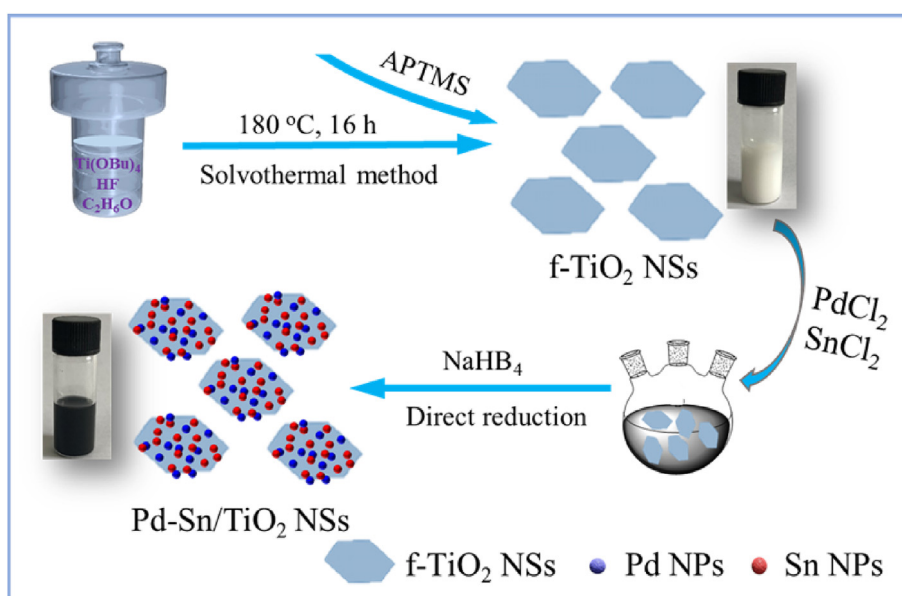

Fig. 1. Schematic diagram for the preparation of Pd—Sn/TiO_2 NSs.

as-prepared catalysts.

3. Results and discussion

3.1. Structure of the Pd–Sn/TiO$_2$ NSs catalyst

The TEM images of the prepared TiO$_2$ NSs are shown in Fig. 2a. Results show that 2D ultrathin TiO$_2$ NSs with molecular-scale thickness can provide abundant active sites for EOR due to larger surface area. However, under the influence of the certain synergistic effect between Sn and TiO$_2$ NSs [41], Pd and Sn nanoparticles without obvious aggregation were co-reduced on the surface of 2D nanosheets (Fig. 2b). The surface roughness of the NSs is relevant to the uniform deposition of Pd and Sn on TiO$_2$ NSs. Meanwhile, the average diameter of Pd–Sn NPs (Fig. S1) is 5.0 ± 0.4 nm calculated by counting 100 random Pd–Sn NPs, as demonstrated by the histogram. The chemical composition of TiO$_2$ NSs and Pd–Sn/TiO$_2$ NSs determined by EDX are shown in Fig. 2a–b. The Si peak roots from glass slides. Meanwhile, the peaks of Ti and O describe adequately TiO$_2$ NSs. The peaks of Pd and Sn belong to the Pd and Sn nanoparticles on the surface of TiO$_2$ NSs.

Meanwhile, as verified by HR-TEM image and EDX mapping (Fig. 2c), Pd and Sn NPs are evenly dispersed on TiO$_2$ NS. The dispersion of nanoparticles can not only help to obtain high specific activity electrocatalysts but also enhance catalyst utilization [19]. Besides, the EDX mapping indicated that Pd and Sn NPs alloy are partially formed. It is worth noting that the surface of TiO$_2$ NS capped by Pd and Sn are still partly exposed. As shown in Fig. 2d, Pd and Sn with interplanar lattice fringe spacing of 0.224 nm and 0.291 nm, respectively. Consistent with what spacing of (111) plane of rutile Pd and the spacing of plane (110) of Sn. The above results demonstrate that the prepared sample has high crystallinity, which makes the sample has good alkali resistance or acid resistance. Therefore, the catalyst may have excellent stability in the EOR
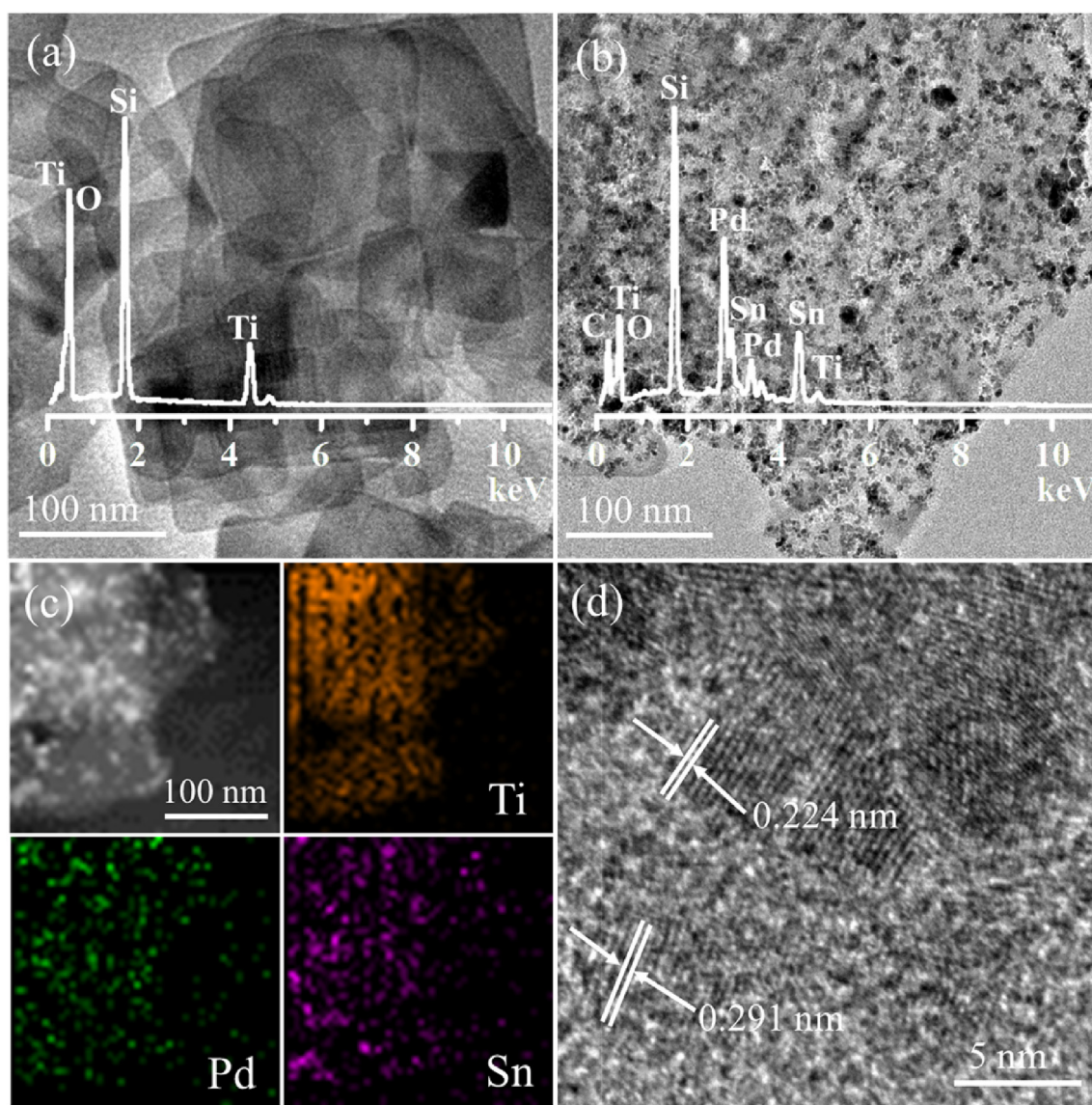

Fig. 2. TEM and EDX images of TiO$_2$ NSs (a), Pd–Sn/TiO$_2$ NSs (b), HAADF-STEM and EDX mapping images of Pd–Sn/TiO$_2$ NSs (c) and HRTEM images of Pd–Sn/TiO$_2$ NSs (Pd: Sn = 1 : 0.6) (d) with interplanar lattice fringe spacing.

[51,52].

3.2. XRD and XPS characterizations of catalysts

X-ray diffraction (XRD) pattern of the TiO$_2$ NSs (Fig. 3a) indicated the synthesized samples are crystallized and in a pure anatase phase. And a novel 2-dimension structure TiO$_2$ NSs can expose more active sites and have higher resistance CO poisoning ability [53,54]. Meanwhile, the XRD patterns of the prepared Pd−Sn/TiO$_2$ NSs catalysts with different Pd/Sn atomic ratios and controlled samples. Among them, the Pd$_1$-Sn$_x$/TiO$_2$ NSs can be observed that all samples are *fcc* structure, the 2θ values of which are 40.1°, 46.6°, 68.1°, 82.1° and 86.6°, corresponding Pd crystal planes (JCPDS "card no." 46−1043) [55]. Compared with the standard diffraction peaks, the binary of Pd$_1$-Sn$_x$/TiO$_2$ NSs shows slightly negative displacement, which indicates that Pd lattice is modified by adding Sn. And the (331) and (220) crystal planes of Pd were observed to become inconspicuous and almost disappear, which can be assigned to the insertion of Sn with the larger atomic radius into the Pd lattice. The lattice expansion indicates that there was the partial alloy forming between Pd and Sn. With the increase of Sn concentration in the catalysts, the decline of the lattice parameter reveals alloy formation between Pd and Sn owing to the partial substitution of Pd by Sn [56,57]. Meanwhile, the lattice parameters of Pd in the Pd−Sn/TiO$_2$ NSs increased so that the diffraction peak had a negative deviation [58–61]. By comparing the XRD spectra of Pd/TiO$_2$ NSs, Pd−Sn and Pd/C (JM), a slight decline of the lattice parameter of Pd can also be found, indicating there is partial alloy between Pd and Sn. However, there are no distinct diffraction peaks in regard to Sn or SnO$_x$ appear in the XRD pattern, implying that the Sn exists in amorphous state. The peaks of the prepared Pd−Sn/TiO$_2$ NSs did not shift significantly, which is consistent with the results in the literature [3,12], indicating that Pd

and Sn were jointly reduced and the partial alloy was formed in this experiment. Moreover, The metal interaction between Pd and Sn allows ordering effect to resist leaching of specific elements from the system and ensure the uniformity of active sites on the catalyst so that the catalyst have excellent stability [29,36]. At the same time, the crystallinity of the sample decreases because of the loading of Pd, which may reduce the catalytic activity and stability of Pd$_1$-Sn$_x$/TiO$_2$ NSs. By quantitative phase analysis, the suitable fitting atomic ratio of Pd/Sn is about 1.67%.

The surface components and valence states of the prepared Pd−Sn/TiO$_2$ NSs were explored by XPS. The XPS wide scan spectra confirmed Pd (3d) and Sn (3d) along with SiO$_2$, O (1s) and C (1s) (Fig. 3b). Only Pd (3d) and Sn (3d) were presented to emphasize and explain the surface chemistry.

Fig. 3c shows the regional states of the horizontal range of Pd 3d and Sn 3d of the prepared Pd−Sn/TiO$_2$ NSs catalyst. The bond energies corresponding to the metal state of Pd in the Pd 3d$_{5/2}$ orbital and Pd 3d$_{3/2}$ orbital are 334.9 eV and 340.2 eV respectively. And the bond energies corresponding to the oxidation state of Pd are 335.6 eV and 340.9 eV, indicating that Pd elements mainly exist in the metal state in the prepared compounds. According to the integral area of the two valence states of Pd, the composition ratio of metallic Pd/oxidative Pd is about 1.5:1. Compared with pure Pd, the 3d peak of Pd has a positive shift (0.7 V) in Pd$_1$−Sn$_{0.6}$/TiO$_2$ NSs, in line with the charge transfer between Pd and Sn in the catalyst [16].

Fig. 3d shows that the two peaks at 486.7 eV and 495.2 eV correspond to Sn 3d$_{5/2}$ and Sn 3d$_{3/2}$ of the oxidation state, respectively. The two peaks at 485.8 eV and 494.3 eV correspond to the Sn 3d$_{5/2}$ and Sn 3d$_{3/2}$ metal orbitals, respectively. Hence, most of the Sn on the surface of Pd$_1$−Sn$_{0.6}$/TiO$_2$ NSs nanocomposite has been oxidized due to the oxophilic metal nature of the Sn atoms [33]. It is obvious that Sn element mainly exists on the surface of Pd$_1$−Sn$_{0.6}$/TiO$_2$ NSs in the form of oxygen-containing species where
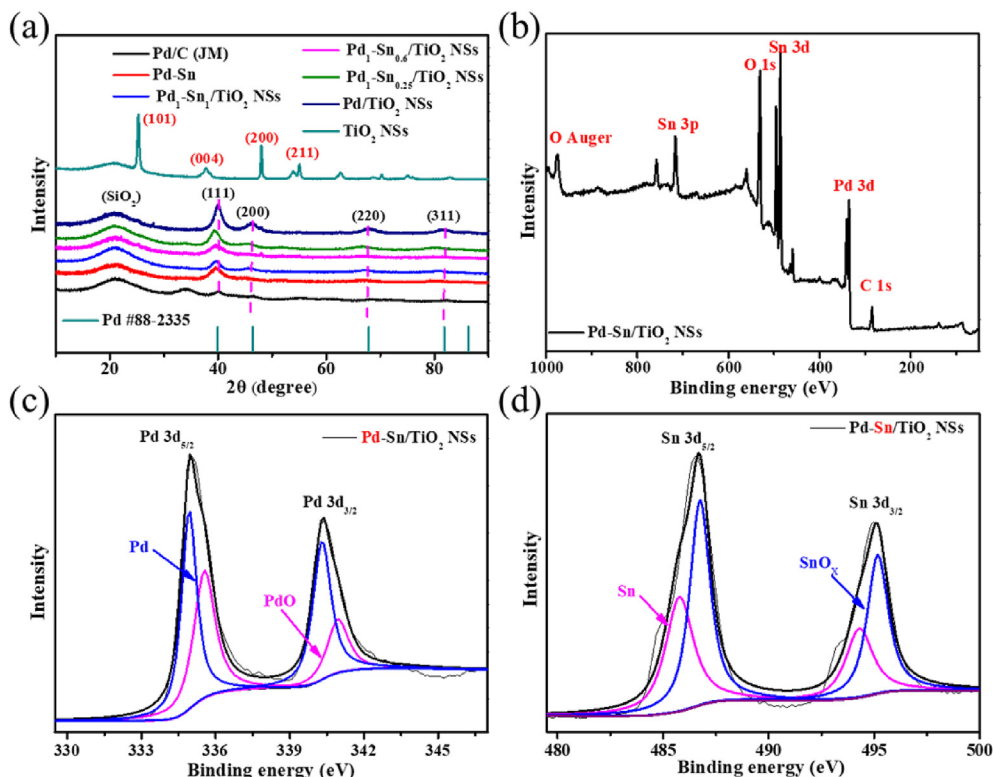

Fig. 3. (a) XRD patterns of Pd$_1$Sn$_x$/TiO$_2$ NSs and control samples, (b) Pd−Sn/TiO$_2$ NSs, (c) Pd 3 d and (d) Sn 3 d XPS spectra of the Pd−Sn/TiO$_2$ NSs nanocomposites.

Sn plays an important role in the oxidation of CO ads to CO_2 and acetaldehyde to acetic acid [2,13]. Therefore, the charge transfer interaction between Pd and Sn significantly changes the electronic state of the Pd atom, which may enhance the electrocatalytic activity and stability.

3.3. Electrochemical characterization

Fig. 4a shows the typical CVs of Pd_1-Sn_x/TiO_2 NSs (with different atomic ratios) and Pd/C (JM, wt%$_{(Pd)}$ = 50%) which were obtained between −0.8 and 0.6 V. The activation peak of water on Pd surface occurred at the −0.5 V, and in this way the oxygen species were produced [16]. For Pd_1−$Sn_{0.25}$/TiO_2 NSs, Pd_1−$Sn_{0.6}$/TiO_2 NSs, Pd_1−Sn_1/TiO_2 NSs and Pd/C catalysts, the activation peaks of water

appeared at −0.3, −0.37, −0.23 and −0.33 V, respectively. The potential has an obvious peak value between −0.6 ~ −0.2 V, which is caused by the reduction of PdO to Pd [38,42]. Furthermore, results show that all peak values of Pd_1-Sn_x/TiO_2 NSs were more negative than that of Pd/C (JM), which is mainly put down to the fact that the activation process to generate OH^- oxidation adsorption CO requires a high potential on Pd. Moreover, the potential of Pd−Sn/TiO_2 NSs slightly ascent to positive than that of Pd/TiO_2 NSs, Pd−Sn and Pd−Sn/C catalysts (Fig. S4a) which is putted down to charge transfer for the synergistic effect between Sn and TiO_2 NSs. Compared with Pd−Sn and Pd−Sn/C, the PdO reduction potential of Pd/TiO_2 NSs is lower. This phenomenon indicates that TiO_2 NSs bring about more significant improvement on the catalytic performance in contrast with oxophilic Sn.
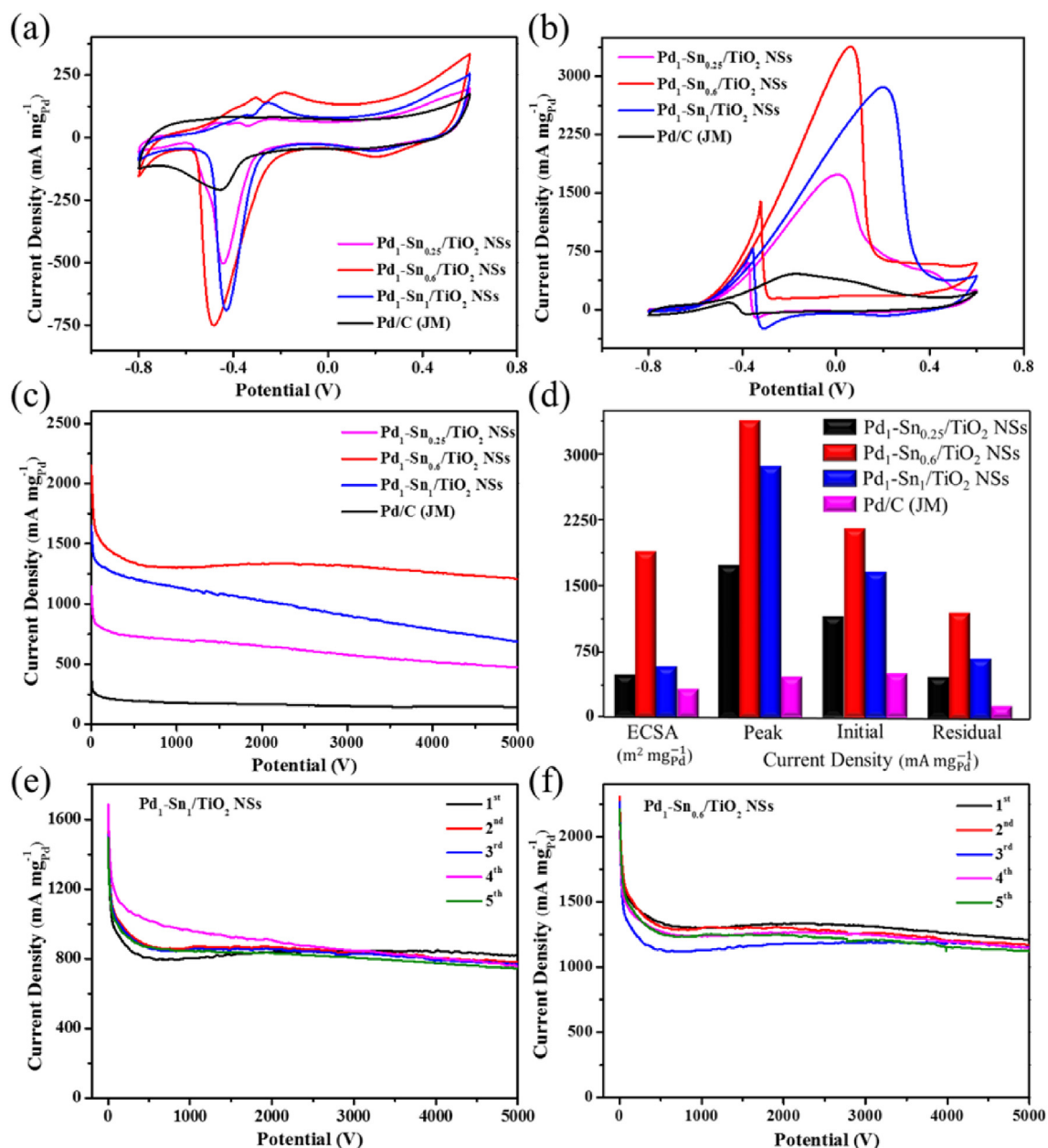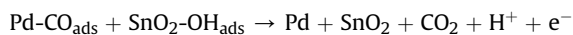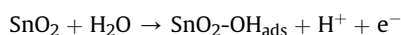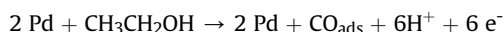

Fig. 4. CV of Pd_1-Sn_x/TiO_2 NSs and Pd/C (JM) measured in 1 M NaOH (a) and 1 M NaOH + 1 M C_2H_5OH (b) at a scan rate of 50 mV s^{-1}. (c) CA of Pd_1-Sn_x/TiO_2 NSs and Pd/C (JM) measured in 1 M NaOH + 1 M C_2H_5OH at −0.2 V vs. Ag/AgCl. (d) The detailed date of ECSA, Peak Current Density, Initial, and Residual Current Density after 5000 s test for Pd_1−$Sn_{0.25}$/TiO_2 NSs, Pd_1−$Sn_{0.6}$/TiO_2 NSs, Pd_1−Sn_1/TiO_2 NSs and Pd/C (JM). (e) Pd_1−Sn_1/TiO_2 NSs and (f) Pd_1−$Sn_{0.6}$/TiO_2 NSs catalysts obtained in 1 M NaOH + 1 M C_2H_5OH at −0.2 V vs. Ag/AgCl.

To verify that the amendment of Pd−Sn on TiO_2 NSs provided more active sites for EOR, the electrochemical active surface area (ECSA) of Pd was calculated from the reduction peak region of PdO [62]. The ECSA values of Pd_1−$Sn_{0.25}$/TiO_2 NSs, Pd_1−$Sn_{0.6}$/TiO_2 NSs, Pd_1−Sn_1/TiO_2 NSs and Pd/C (JM) catalysts are 478.6, 1887.2, 578.75 and 327.12 mA mg_{Pd}^{-1}, respectively. The results are as the following sequence: Pd_1−$Sn_{0.6}$/TiO_2 NSs > Pd_1−Sn_1/TiO_2 NSs > Pd_1−$Sn_{0.25}$/TiO_2 NSs > Pd/C (JM). The ESCA values indicate that the Pd/Sn loading ratio has a certain influence on the electrocatalytic performance. The ECSA of Pd_1−$Sn_{0.6}$/TiO_2 NSs is much larger than Pd/TiO_2 NSs, Pd−Sn and Pd−Sn/C, clearly confirming the strong interaction of Pd−Sn nanoparticles and TiO_2 NSs. Adding Sn can make CO oxidize to CO_2 in Pd−Sn/TiO_2 NSs which has high CO anti-poisoning in the kinetic process of EOR. Besides, a suitable proportion between Pd and Sn in the catalysts is also important. Combining elemental mapping and ECSA analysis, the Sn NPs have been uniformly distributed around Pd, which is formed for the bi-functional effect between Pd and Sn [16,46,63,64]. Sn reduces the oxidation potential of the provided OH_{ads} group to remove the CO_{ads} in the adsorption state by the following pathway [11,33,65]:

$$2\ Pd + CH_3CH_2OH \rightarrow 2\ Pd + CO_{ads} + 6H^+ + 6\ e^-$$

$$SnO_2 + H_2O \rightarrow SnO_2\text{-}OH_{ads} + H^+ + e^-$$

$$Pd\text{-}CO_{ads} + SnO_2\text{-}OH_{ads} \rightarrow Pd + SnO_2 + CO_2 + H^+ + e^-$$

Thus, the electronic effect of Pd and Sn could enhance the catalytic activity of Pd−Sn/TiO_2 NSs catalysts.

Fig. 4b exhibits CV curves of the Pd_1-Sn_x/TiO_2 NSs and Pd/C (JM) tested in an N_2-saturated 1.0 M NaOH + 1.0 M C_2H_5OH solution. Two typical characteristic peaks can be seen from the CV curves. A significant peak is observed in −0.2−0.4 V, and another peak is observed in −0.1−0.2 V, showing the oxidation capacity of ethanol

to acetate. The electrochemical activity of the Pd_1-Sn_x/TiO_2 NSs is higher than that of commercial Pd/C (JM). Notably, the peak current density of Pd_1−$Sn_{0.6}$/TiO_2 NSs, Pd_1−Sn_1/TiO_2 NSs and Pd_1−$Sn_{0.25}$/TiO_2 NSs are approximately 3381, 2862, 1735 mA mg_{Pd}^{-1}, respectively, which are 7.3, 6.2 and 3.8 times than that of Pd/C (JM) (458 mA mg_{Pd}^{-1}). In addition, the Pd_1−$Sn_{0.6}$/TiO_2 NSs is much higher than that of Pd/TiO_2 NSs (483 mA mg_{Pd}^{-1}), Pd−Sn (446.5 mA mg_{Pd}^{-1}) and Pd_1−$Sn_{0.6}$/C (331.8 mA mg_{Pd}^{-1}) (Fig. S4b), implying that the existence of Sn and TiO_2 NSs could boost the catalytic activity toward EOR. Actually, the TiO_2 NSs can provide enough specific surface area and activity sites so that Pd−Sn nanoparticles can be uniformly anchored on 2D-nanostructured TiO_2 NSs. Furthermore, the onset potential is similar to that of CO oxidation, demonstrating that the second peak is due to the oxidative desorption of the unoxidized intermediate products [66−68]. The catalytic activity of Pd_1−$Sn_{0.6}$/TiO_2 NSs was evaluated by the CV test (Figs. S2a−b). The current density of Pd_1−$Sn_{0.6}$/TiO_2 NSs increased gradually during the initial few cycles of scanning due to the fresh catalyst possesses abundant active sites for EOR. After 40 cycles of scanning, the current density still showed up trend, indicating the catalytic activity and durable stability was enhanced.

The stability test of Pd_1-Sn_x/TiO_2 NSs and Pd/C (JM) is performed by chronoamperometry (CA). The initial current density (Fig. 4c) of the prepared Pd−Sn/TiO_2 NSs catalyst was much higher than that of Pd/C (JM), because Pd−Sn/TiO_2 NSs expose plentiful active sites in the initial stage. Moreover, the activity of the prepared Pd−Sn/TiO_2 NSs catalyst still kept at a high level after the 5000 s I-t test. In 0−40 s, the abundant exposed active sites resulted in a high initial current density. In 40−500 s, the rapid descent of the current density is ascribed to an increasing ratio of CO_{ads} and oxygen donating species in the few seconds [3,58].

Among them, the Sn on the prepared Pd_1−$Sn_{0.6}$/TiO_2 NSs catalyst can enhance the anti-poisoning ability to the intermediate medium such as CO due to the electronic effect, thus promoting the
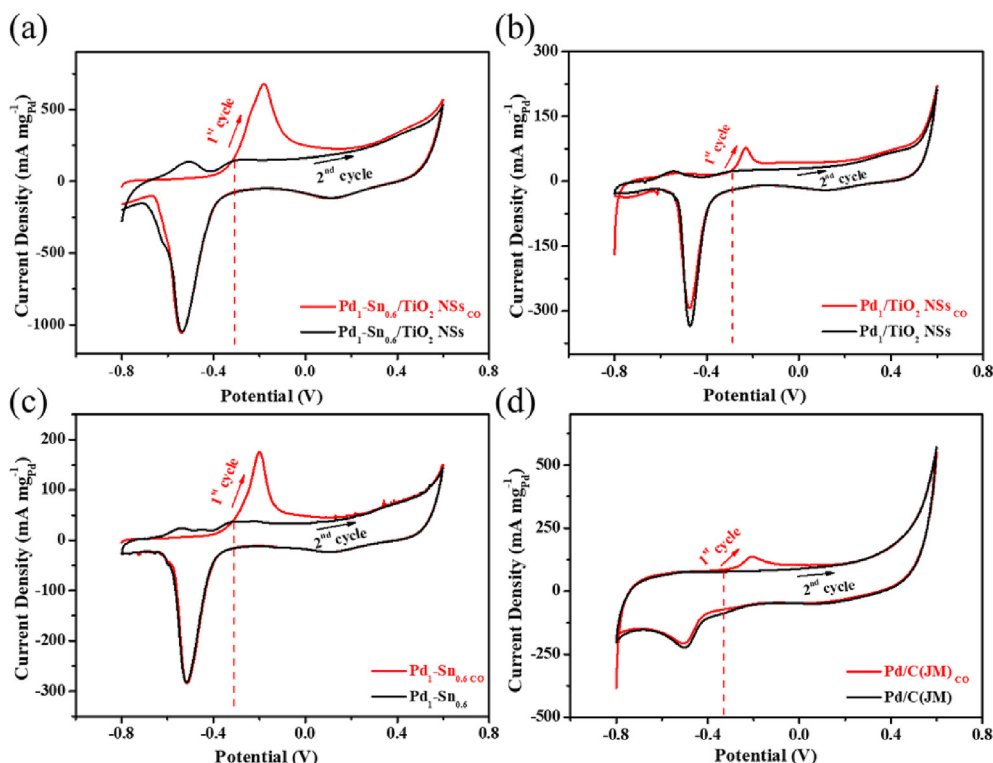

Fig. 5. CO stripping curves of Pd_1−$Sn_{0.6}$/TiO_2 NSs catalysts (a), Pd/TiO_2 NSs (b), Pd−Sn (c) and Pd/C (d) in 1 M NaOH.

kinetics of ethanol oxidation [12,53]. Meanwhile, Fig. 4d shows the residual current density of $Pd_1-Sn_{0.6}/TiO_2$ NSs, Pd_1-Sn_1/TiO_2 NSs and $Pd_1-Sn_{0.25}/TiO_2$ NSs are 1207, 685 and 472 mA mg_{Pd}^{-1}, which are 8.5, 4.8 and 3.3 times than that of Pd/C (JM) (142 mA mg_{Pd}^{-1}), respectively. After the 5000 s durability test, the partially deactivated catalysts, such as Pd_1-Sn_1/TiO_2 NSs (Fig. 4e) and $Pd_1-Sn_{0.6}/TiO_2$ NSs (Fig. 4f) could be easily reactivated with several CV cycles in 1.0 M NaOH. It is found that the current density can still be maintained at a high level. Due to the sample in the alkaline solution eliminates the carbonaceous species absorbed on Pd surface, the active sites can be re-exposed and the aggregation of NPs and the dissolution of Pd in the NaOH solution. The performance of $Pd_1-Sn_{0.6}/TiO_2$ NSs decay only 20% after 300 consecutive sweeps of CVs (Fig. S3) although the catalyst have been kept in the air for 7 months. It proves in further that the $Pd_1-Sn_{0.6}/TiO_2$ NSs have the good long-term cycle stabilities of catalysts.

In addition, it can be seen clearly in (Figs. S4c−d) that the residual current of $Pd_1-Sn_{0.6}/TiO_2$ NSs is much greater than that of Pd−Sn, Pd/C (JM) and Pd−Sn/C. The reaction activity of the catalyst can be adjusted by changing the preparation conditions such as the metal loading and the carrier. It is clear that the crystal lattice surface (001) of TiO_2 NSs affects the catalyst performance from the analysis above. And the interface effect is formed on the crystal lattice surface (001), which greatly improves the stability and activity of the catalyst [8,69].

During process of ethanol electrooxidation on the surface of the catalyst, the CO_{ads} affects the mass activity and long-term stability of the catalyst. To further explore the anti-poisoning ability of catalyst, CO stripping voltammograms of $Pd_1-Sn_{0.6}/TiO_2$ NSs catalysts are plotted in Fig. 5a. Evidently, the CO oxidation peaks of the $Pd_1-Sn_{0.6}/TiO_2$ NSs at about −0.32 V to −0.15 V during the first CV scan cycle can be attributed to the adsorbed CO (CO_{ads}) on catalyst [58,70]. Subsequently, the second CVs go with by the vanishing of CO oxidation peaks due to the removal of adsorbed CO (CO_{ads}). The anti-poisoning ability of CO can be seen from the peak sharpness and the area of the oxidation peak of CO [3]. So it is not hard to find in Fig. 5a−d that $Pd_1-Sn_{0.6}/TiO_2$ NSs > Pd/TiO_2 NSs > Pd−Sn > Pd/C (JM). Moreover, Pd/TiO_2 NSs (Fig. 5b) and Pd -Sn (Fig. 5c) were compared with Pd/C (JM) (Fig. 5d) in the CO stripping voltammetry indicating the harder exclusion of CO_{ads} on Pd/TiO_2 NSs and Pd−Sn. This could be concluded that the combination of Pd and Sn can decrease the initial potential of the catalyst reaction and the oxidation of adsorbed CO. These results indicated that the addition of Sn may alleviate the CO poisoning of Pd-based electrocatalysts. At the same time, the TiO_2 NSs catalyst carrier has a great promoting effect on the anti-CO poisoning ability. The main function of the carrier is to provide enough active sites, so that Pd and Sn can play an important catalytic role in DEFC.

4. Conclusions

In summary, Pd−Sn/TiO_2 NSs catalyst with high activity for EOR was successfully synthesized by chemical reduction method. Pd−Sn/TiO_2 NSs nano-catalyst has good activity and durability, mainly because of the electronic effect between Sn and Pd and the fact that TiO_2 NSs (001) surface provides enough active sites for the metals to be loaded on uniformly. Meanwhile, the current density of the catalytic oxidation activity of Pd−Sn/TiO_2 NSs was 7.2 times than that of Pd/C(JM), and the residual current density (1207 mA mg_{Pd}^{-1}) was 8.5 times higher than that of Pd/C(JM) (142 mA mg_{Pd}^{-1}) after the 5000 s I-t test. At the same time, the prepared catalyst showed excellent CO anti-poisoning ability towards EOR. All the results show that Pd−Sn/TiO_2 NSs is a promising electrocatalyst with superior performance for DEFCs.

Appendix A. Supplementary data

Supplementary data to this article can be found online at https://doi.org/10.1016/j.electacta.2019.134588.

References

[1] E. Antolini, E.R. Gonzalez, Alkaline direct alcohol fuel cells, J. Power Sources 195 (2010) 3431−3450.
[2] J. Kim, T. Momma, T. Osaka, Cell performance of Pd−Sn catalyst in passive direct methanol alkaline fuel cell using anion exchange membrane, J. Power Sources 189 (2009) 999−1002.
[3] X. Wang, F. Zhu, Y. He, M. Wang, Z. Zhang, Z. Ma, R. Li, Highly active carbon supported ternary $PdSnPt_x$ (x = 0.1-0.7) catalysts for ethanol electrooxidation in alkaline and acid media, J. Colloid Interface Sci. 468 (2016) 200−210.
[4] C. Chen, L. Jin, H. Shang, T. Song, F. Gao, Y. Zhang, C. Wang, C. Wang, Y. Du, Monodispersed bimetallic platinum-copper alloy nanospheres as efficient catalysts for ethylene glycol electrooxidation, J. Colloid Interface Sci. 551 (2019) 81−88.
[5] F. Gao, Y. Zhang, P. Song, J. Wang, T. Song, C. Wang, L. Song, Y. Shiraishi, Y. Du, Precursor-mediated size tuning of monodisperse PtRh nanocubes as efficient electrocatalysts for ethylene glycol oxidation, J. Mater. Chem. 7 (2019) 7891−7896.
[6] Y.H. Qin, Z.Y. Xiong, J. Ma, L. Yang, Z. Wu, W. Feng, T.L. Wang, W.G. Wang, C.W. Wang, Enhanced electrocatalytic activity and stability of Pd nanoparticles supported on TiO_2 modified nitrogen-doped carbon for ethanol oxidation in alkaline media, Int. J. Hydrogen Energy 42 (2017) 1103−1112.
[7] Y. Wang, C. Du, Y. Sun, G. Han, F. Kong, G. Yin, Y. Gao, Y. Song, The enhanced CO tolerance of platinum supported on FeP Nanosheet for superior catalytic activity toward methanol oxidation, Electrochim. Acta 254 (2017) 36−43.
[8] W. Zhang, Q. Qin, L. Dai, R. Qin, X. Zhao, X. Chen, D. Ou, J. Chen, T.T. Chuong, B. Wu, N. Zheng, Electrochemical reduction of carbon dioxide to methanol on hierarchical Pd/SnO_2 nanosheets with abundant Pd-O-Sn interfaces, Angew. Chem. Int. Ed. 57 (2018) 9475−9479.
[9] F. Gao, Y. Zhang, P. Song, J. Wang, C. Wang, J. Guo, Y. Du, Self-template construction of sub-24 nm PdAg hollow nanodendrites as highly efficient electrocatalysts for ethylene glycol oxidation, J. Power Sources 418 (2019) 186−192.
[10] H. Yang, H. Zou, M. Chen, S. Li, J. Jin, J. Ma, The green synthesis of ultrafine palladium-phosphorus alloyed nanoparticles anchored on polydopamine functionalized graphene used as an excellent electrocatalyst for ethanol oxidation, Inorg. Chem. Front. 4 (2017) 1881−1887.
[11] G. Yang, L.M. Namin, N. Aaron Deskins, X. Teng, Influence of -OH adsorbates on the potentiodynamics of the CO_2 generation during the electro-oxidation of ethanol, J. Catal. 353 (2017) 335−348.
[12] R. Awasthi, R.N. Singh, Optimization of the Pd−Sn−GNS nanocomposite for enhanced electrooxidation of methanol, Int. J. Hydrogen Energy 37 (2012) 2103−2110.
[13] D.D. Tu, B. Wu, B. Wang, C. Deng, Y. Gao, A highly active carbon-supported PdSn catalyst for formic acid electrooxidation, Appl. Catal., B 103 (2011) 163−168.
[14] S. Li, H. Yang, H. Zou, M. Yang, X. Liu, J. Jin, J. Ma, Palladium nanoparticles anchored on NCNTs@NGS with a three-dimensional sandwich-stacked framework as an advanced electrocatalyst for ethanol oxidation, J. Mater. Chem. 6 (2018) 14717−14724.
[15] W. Du, K.E. Mackenzie, D.F. Milano, N.A. Deskins, D. Su, X. Teng, Palladium−tin alloyed catalysts for the ethanol oxidation reaction in an alkaline medium, ACS Catal. 2 (2012) 287−297.
[16] J. Kim, T. Momma, T. Osaka, Synthesis of carbon-supported Pd-Sn catalyst by ultrasonic irradiation for oxygen reduction reaction, J. Power Sources 189 (2009) 909−915.
[17] X. He, L. Ning, A. Zhu, Q. Zhang, Q. Liu, Hollow nanoporous NiPd catalysts with enhanced performance for ethanol electro-oxidation, Int. J. Hydrogen Energy 42 (2017) 24989−25000.
[18] X. Huang, S. Tang, X. Mu, Y. Dai, G. Chen, Z. Zhou, F. Ruan, Z. Yang, N. Zheng, Freestanding palladium nanosheets with plasmonic and catalytic properties, Nat. Nanotechnol. 6 (2011) 28−32.
[19] R. Jiang, D.T. Tran, J.P. McClure, D. Chu, A class of (Pd−Ni−P) electrocatalysts for the ethanol oxidation reaction in alkaline media, ACS Catal. 4 (2014) 2577−2586.
[20] X. Li, X. Wang, M. Liu, H. Liu, Q. Chen, Y. Yin, M. Jin, Construction of Pd-M (M = Ni, Ag, Cu) alloy surfaces for catalytic applications, Nano Res 11 (2017)

780−790.

[21] D. Chen, Z. He, S.E. Pei, L.A. Huang, H. Shao, Y. Jin, J. Wang, Pd nanoparticles supported on N and P dual-doped graphene as an excellent composite catalyst for methanol electro-oxidation, J. Alloy. Comp. 785 (2019) 781−788.

[22] Y. Li, C. Cheng, S. Bai, L. Jing, Z. Zhao, L. Liu, The performance of Pd-rGO electro-deposited PVDF/carbon fiber cloth composite membrane in MBR/MFC coupled system, Chem. Eng. J. 365 (2019) 317−324.

[23] Y. Zhang, F. Gao, P. Song, J. Wang, J. Guo, Y. Shiraishi, Y. Du, Glycine-assisted fabrication of N-doped graphene-supported uniform multipetal PtAg nanoflowers for enhanced ethanol and ethylene glycol oxidation, ACS Sustain. Chem. Eng. 7 (2019) 3176−3184.

[24] H. Yang, S. Li, S. Shen, Z. Jin, J. Jin, J. Ma, Unraveling the cooperative synergy of palladium/tin oxide/aniline-functionalized carbon nanotubes enabled by layer-by-layer synthetic strategy for ethanol electrooxidation, ACS Sustain. Chem. Eng. 7 (2019) 10008−10015.

[25] W. Wang, Y. Kang, Y. Yang, Y. Liu, D. Chai, Z. Lei, PdSn alloy supported on phenanthroline-functionalized carbon as highly active electrocatalysts for glycerol oxidation, Int. J. Hydrogen Energy 41 (2016) 1272−1280.

[26] P. Raghavendra, G. Vishwakshan Reddy, R. Sivasubramanian, P. Sri Chandana, L. Subramanyam Sarma, Reduced graphene oxide-supported Pd@Au bimetallic nano electrocatalyst for enhanced oxygen reduction reaction in alkaline media, Int. J. Hydrogen Energy 43 (2018) 4125−4135.

[27] H. Xu, B. Yan, K. Zhang, C. Wang, J. Zhong, S. Li, P. Yang, Y. Du, Facile synthesis of Pd-Ru-P ternary nanoparticle networks with enhanced electrocatalytic performance for methanol oxidation, Int. J. Hydrogen Energy 42 (2017) 11229−11238.

[28] H. Zhang, Y. Song, Z. Liang, X. Zhang, B. Xu, J. Guo, A novel Sn/SnO/graphene triple core-shell heterogeneous catalyst for oxygen reduction reaction, Inorg. Chem. Commun. 96 (2018) 101−105.

[29] A.B. Suryamas, G.M. Anilkumar, S. Sago, T. Ogi, K. Okuyama, Electrospun Pt/SnO₂ nanofibers as an excellent electrocatalysts for hydrogen oxidation reaction with ORR-blocking characteristic, Catal. Commun. 33 (2013) 11−14.

[30] W. Kang, H. Guo, A. Varma, Noble-metal-free NiCu/CeO₂ catalysts for H₂ generation from hydrous hydrazine, Appl. Catal., B 249 (2019) 54−62.

[31] A.S. Brayko, A.B. Shigarov, V.A. Kirillov, V.V. Kireenkov, N.A. Kuzin, V.A. Sobyanin, P.V. Snytnikov, V.V. Kharton, Methane partial oxidation over porous nickel monoliths: the effects of NiO-MgO loading on microstructural parameters and hot-spot temperature, Mater. Lett. 236 (2019) 264−266.

[32] R.M. Modibedi, T. Masombuka, M.K. Mathe, Carbon supported Pd−Sn and Pd−Ru−Sn nanocatalysts for ethanol electro-oxidation in alkaline medium, Int. J. Hydrogen Energy 36 (2011) 4664−4672.

[33] R. Wang, Z. Liu, Y. Ma, H. Wang, V. Linkov, S. Ji, Heterostructure core PdSn−SnO₂ decorated by Pt as efficient electrocatalysts for ethanol oxidation, Int. J. Hydrogen Energy 38 (2013) 13604−13610.

[34] M.R. Miah, J. Masud, T. Ohsaka, Kinetics of oxygen reduction reaction at electrochemically fabricated tin-palladium bimetallic electrocatalyst in acidic media, Electrochim. Acta 56 (2010) 285−290.

[35] X. Lu, Y. Wu, X. Yuan, H. Wang, An integrated CO₂ electrolyzer and formate fuel cell enabled by a reversibly restructuring Pb-Pd bimetallic catalyst, Angew. Chem. Int. Ed. 58 (2019) 4031−4035.

[36] S. Verdier, Pd−Sn/Al₂O₃ catalysts from colloidal oxide synthesis I. Preparation of the catalysts, J. Catal. 218 (2003) 280−287.

[37] H. Yang, Z. Yu, S. Li, Q. Zhang, J. Jin, J. Ma, Ultrafine palladium-gold-phosphorus ternary alloyed nanoparticles anchored on ionic liquids-noncovalently functionalized carbon nanotubes with excellent electrocatalytic property for ethanol oxidation reaction in alkaline media, J. Catal. 353 (2017) 256−264.

[38] J. Kim, J.E. Park, T. Momma, T. Osaka, Synthesis of Pd−Sn nanoparticles by ultrasonic irradiation and their electrocatalytic activity for oxygen reduction, Electrochim. Acta 54 (2009) 3412−3418.

[39] Y. Hu, A. Zhu, C. Zhang, Q. Zhang, Q. Liu, Microwave-assisted synthesis of double-shell PtRu/TiO₂ catalyst towards methanol electro-oxidation, Int. J. Hydrogen Energy 40 (2015) 15652−15662.

[40] L. Ning, A. Zhu, M. Deng, Q. Zhang, Q. Liu, Novel H-PdSnNi catalyst with enhanced ethanol electrooxidation performance in alkaline medium, Electrochim. Acta 259 (2018) 1145−1153.

[41] X. Liu, X. Wang, J. Wu, A. Zhu, Q. Zhang, Q. Liu, Synergy effects between Sn and SiO₂ on enhancing the anti-poison ability to CO for ethanol electrooxidation, Electrochim. Acta 302 (2019) 145−152.

[42] X. Liu, L. Ning, M. Deng, J. Wu, A. Zhu, Q. Zhang, Q. Liu, Self-recoverable Pd-Ru/TiO₂ nanocatalysts with ultrastability towards ethanol electrooxidation, Nanoscale 11 (2019) 3311−3317.

[43] X. Zou, R. Silva, X. Huang, J.F. Al-Sharab, T. Asefa, A self-cleaning porous TiO₂-Ag core-shell nanocomposite material for surface-enhanced Raman scattering, Chem. Commun. 49 (2013) 382−384.

[44] J.S. Chen, L.A. Archer, X. Wen Lou, SnO₂ hollow structures and TiO₂ nanosheets for lithium-ion batteries, J. Mater. Chem. 6 (2012) 246−254.

[45] L. Gao, S. Li, D. Huang, Y. Shen, M. Wang, ZnO decorated TiO₂ nanosheet composites for lithium ion battery, Electrochim. Acta 182 (2015) 529−536.

[46] H.G. Yang, G. Liu, S.Z. Qiao, C.H. Sun, Y.G. Jin, S.C. Smith, J. Zou, H.M. Cheng, G.Q. (Max) Lu, Solvothermal synthesis and photoreactivity of anatase TiO₂ nanosheets with dominant {001} facets, J. Am. Chem. Soc. 131 (2009) 4078−4083.

[47] M. Li, Y. Chen, W. Li, X. Li, H. Tian, X. Wei, Z. Ren, G. Han, Ultrathin anatase TiO₂ nanosheets for high-performance photocatalytic hydrogen production, Small 13 (2017) 1604115.

[48] J.S. Chen, X.W. Lou, Anatase TiO₂ nanosheet: an ideal host structure for fast and efficient lithium insertion/extraction, Electrochem. Commun. 11 (2009) 2332−2335.

[49] J. Li, H. Zhou, H. Zhuo, Z. Wei, G. Zhuang, X. Zhong, S. Deng, X. Li, J. Wang, Oxygen vacancies on TiO₂ promoted the activity and stability of supported Pd nanoparticles for the oxygen reduction reaction, J. Mater. Chem. 6 (2018) 2264−2272.

[50] L. Nie, P. Zhou, J. Yu, M. Jaroniec, Deactivation and regeneration of Pt/TiO₂ nanosheet-type catalysts with exposed (001) facets for room temperature oxidation of formaldehyde, J. Mol. Catal. A Chem. 390 (2014) 7−13.

[51] Q. Dong, Q. Wu, D. Mei, Y. Shao, Y. Wang, J. Liu, H. Li, L. Hong, Multifunctional Pd-Sn electrocatalysts enabled by in situ formed SnOₓ and TiC triple junctions, Nano Energy 53 (2018) 940−948.

[52] L. Gao, W. Yue, S. Tao, L. Fan, Novel strategy for preparation of graphene-Pd, Pt composite, and its enhanced electrocatalytic activity for alcohol oxidation, Langmuir 29 (2013) 957−964.

[53] F. Wu, Z. Wang, X. Li, H. Guo, Simple preparation of petal-like TiO₂ nanosheets as anode materials for lithium-ion batteries, Ceram. Int. 40 (2014) 16805−16810.

[54] K. Liu, X. Yan, P. Zou, Y. Wang, L. Dai, Large size Pd NPs loaded on TiO₂ as efficient catalyst for the aerobic oxidation of alcohols to aldehydes, Catal. Commun. 58 (2015) 132−136.

[55] Q. Liu, Y.R. Xu, A.J. Wang, J.J. Feng, A single-step route for large-scale synthesis of core−shell palladium@platinum dendritic nanocrystals/reduced graphene oxide with enhanced electrocatalytic properties, J. Power Sources 302 (2016) 394−401.

[56] A. Brouzgou, S. Song, P. Tsiakaras, Carbon-supported PdSn and Pd₃Sn₂ anodes for glucose electrooxidation in alkaline media, Appl. Catal., B 158−159 (2014) 209−216.

[57] D.D. Tu, B. Wu, B. Wang, C. Deng, Y. Gao, A highly active carbon-supported PdSn catalyst for formic acid electrooxidation, Appl. Catal., B 103 (2011) 163−168.

[58] S. Salome, A.M. Ferraria, A.M.B. do Rego, F. Alcaide, O. Savadogo, R. Rego, Enhanced activity and durability of novel activated carbon-supported PdSn heat-treated cathode catalyst for polymer electrolyte fuel cells, Electrochim. Acta 192 (2016) 268−282.

[59] T. Ramulifho, K.I. Ozoemena, R.M. Modibedi, C.J. Jafta, M.K. Mathe, Electrocatalytic oxidation of ethylene glycol at palladium-bimetallic nanocatalysts (PdSn and PdNi) supported on sulfonate-functionalised multi-walled carbon nanotubes, J. Electroanal. Chem. 692 (2013) 26−30.

[60] H. Mao, L. Wang, P. Zhu, Q. Xu, Q. Li, Carbon-supported PdSn−SnO₂ catalyst for ethanol electro-oxidation in alkaline media, Int. J. Hydrogen Energy 39 (2014) 17583−17588.

[61] F. Li, Q. Shao, M. Hu, Y. Chen, X. Huang, Hollow Pd−Sn nanocrystals for efficient direct H₂O₂ synthesis: the critical role of Sn on structure evolution and catalytic performance, ACS Catal. 8 (2018) 3418−3423.

[62] K. Bian, Y. Li, W. Xue, L. Luo, L. Li, Y. He, C. Cong, J. An, D. Gao, Direct synthesis of ultralong platinum nanowires with prominent electrocatalytic performance using lanreotide biotemplate, Nanotechnology 30 (2019) 085401.

[63] L. Bu, N. Zhang, S. Guo, X. Zhang, J. Li, J. Yao, T. Wu, G. Lu, J.Y. Ma, D. Su, X. Huang, Biaxially strained PtPb/Pt core/shell nanoplate boosts oxygen reduction catalysis, Science 354 (2016) 1410−1414.

[64] C. He, J. Tao, Pt loaded two-dimensional TaC-nanosheet/graphene hybrid as an efficient and durable electrocatalyst for direct methanol fuel cells, J. Power Sources 324 (2016) 317−324.

[65] Y. Wu, C. Wang, L. Zou, Q. Huang, H. Yang, Incorporation of cobalt into Pd₂Sn intermetallic nanoparticles as durable oxygen reduction electrocatalyst, J. Electroanal. Chem. 789 (2017) 167−173.

[66] L. Lin, M. Yuan, Z. Sun, H. Li, C. Nan, G. Sun, S. Ma, The in situ growth of ultrathin Fcc-NiPt nanocrystals on graphene for methanol and formic acid oxidation, Dalton Trans. 47 (2018) 15131−15140.

[67] G. Wang, J. Jiang, Q. Huang, Y. Zhou, Z. Zou, H. Yang, Interconnected nanoparticle-stacked platinum-based nanosheets as active cathode electrocatalysts for passive direct methanol fuel cells, J. Electroanal. Chem. 828 (2018) 50−58.

[68] L.H. Yuwen, F. Xu, B. Xue, Z. Luo, Q. Zhang, B. Bao, S. Su, L. Weng, W. Huang, L. Wang, General synthesis of noble metal (Au, Ag, Pd, Pt) nanocrystal modified MoS₂ nanosheets and the enhanced catalytic activity of Pd−MoS₂ for methanol oxidation, Nanoscale 6 (2014) 5762−5769.

[69] J. Bai, G.R. Xu, S.H. Xing, J.H. Zeng, J.X. Jiang, Y. Chen, Hydrothermal synthesis and catalytic application of ultrathin rhodium nanosheet nanoassemblies, ACS Appl. Mater. Interfaces 8 (2016) 33635−33641.

[70] G. Sun, L. Zhou, J. Li, J. Tang, Y. Wang, Human hair-derived graphene-like carbon nanosheets to support Pt nanoparticles for direct methanol fuel cell application, RSC Adv. 5 (2015) 71980−71987.